Proceedings of the ASME 2020 Fluids Engineering Division Summer Meeting
FEDSM2020
July 13-15, 2020, Virtual, Online

FEDSM2020-20237

DISRUPTION BEHAVIOR OF AGGREGATES IN A ROTATING/OSCILLATING CYLINDRICAL TANK AND IMPLICATIONS FOR PARTICLE TRANSPORT IN THE OCEAN

Yixuan Song, Matthew J. Rau[1]
Department of Mechanical Engineering
The Pennsylvania State University
University Park, PA 16802, USA

ABSTRACT

Particle size and settling speed determine the rate of particulate mass transfer from the ocean surface to the sea bed. Turbulent shear in the ocean can act on large, faster-settling flocculated particles to break them into slower-settling primary particles or sub-aggregates. However, it is difficult to understand the disruption behavior of aggregates and their response to varying shear forces due to the complex ocean environment. A study was conducted to simulate the disruption behavior of marine aggregates in the mixed layer of the ocean. The breakup process was investigated by aggregating and disrupting flocs of bentonite clay particles in a rotating and oscillating cylindrical tank 10 cm in diameter filled with salt water. This laboratory tank, which operated based on an extension of Stokes' second problem inside a cylinder, created laminar oscillating flow superimposed on a constant rotation. This motion allowed the bentonite particles to aggregate near the center of the tank but also exposed large aggregates to high shear forces near the wall. A high-speed camera system was used, along with particle tracking measurements and image processing techniques, to capture the breakup of the large particle aggregates and locate their radial position. The breakup response of large aggregates and the sizes of their daughter particles after breakup were quantified using the facility. The disruption strength of the aggregated particles is presented and discussed relative to their exposure to varying amounts of laminar shear.

Keywords: Disaggregation, aggregation, roller tank, extension to Stokes' second problem, laminar shear

NOMENCLATURE

a	amplitude of oscillation
b	rotation component of wall velocities
r	radial distance from the center of disaggregation tank
t	time
u_θ	velocity of fluid parcel
$u_{\theta,H}$	homogenous part of velocity of fluid parcel
I_1	modified Bessel function of first kind and order one
R	radius of disaggregation tank
γ	shear rate
θ	azimuthal direction
ν	kinematic viscosity
φ	phase angle of oscillation
ω	frequency of oscillation

1. INTRODUCTION

In natural systems like the ocean, particles and flocs (aggregated particles) experience shear forces from the surrounding fluid flow, which can affect how they form and their ultimate size, shape, and density [1]. For example, clay particles and phytoplankton in the ocean can deform or break apart by this fluid shear [2–4]. The magnitude of shear rate γ in the ocean can typically vary from 10^{-2} s^{-1} to 300 s^{-1} [5]. Creating a controlled environment in the laboratory that can generate hydrodynamic shear at these magnitudes, while also allowing measurement of particle aggregation and breakup parameters, is not trivial.

The traditional disaggregation experimental setup typically involves a container with a mixing impeller [2,6,7]. In these systems, the magnitude of shear created is usually high and difficult to determine locally due to the inhomogeneity of the flow [8,9]. Therefore researchers usually quantify shear rates in these devices using average values [2,7,10]. Devices that operate with Taylor-Couette principles have also been effective [6,11], though it is usually difficult to manufacture them. Additionally, flocs in the Taylor-Couette devices can easily interact with the

[1] Contact author: matthew.rau@psu.edu

walls. Such contact with a wall potentially alter the floc size and porosity [12].

Studies of marine aggregated particles (often called marine snow) are unique, in that the aggregated particles are typically quite fragile due to their formation in the marine environment [10]. To mimic natural marine snow particles in the laboratory, researchers often use rolling cylindrical tanks, which cause aggregation of particulate matter through differential sedimentation [13]. Because the fluid motion in these tanks follows solid body rotation (after an initial startup period), we cannot use them for disaggregation studies as there is no way to directly expose the marine snow particles to calibrated shear forces. Typically, researchers must manually extract the marine snow particles and then individually place them in a separate facility for breakup quantification [7]. This manipulation can disaggregate or alter the particles prior to measurement.

Motivated by the need for a controlled experiment in which the aggregation and breakup of individual marine particles could be studied in a finely controlled manner, the authors developed a novel experimental facility [14]. The facility consisted of a cylindrical tank rotating around its axis with a superimposed oscillation to create hydrodynamic shear. In this facility, the velocity and shear rate within the internal fluid can be accurately calculated using the analytical solution developed subsequently by the authors [15]. Unique from Taylor-Couette devices, this disaggregation tank can create conditions where most aggregates do not come into contact with its wall if it is operated by an appropriate boundary condition. These stable operating conditions are discussed in more detail in [14].

This rotating and oscillating tank has several advantages for studying marine particle disaggregation. Because it is based on a rolling cylindrical tank, we can first operate the tank to aggregate particulate matter using solid body rotation in a similar manner to the facilities used to create marine snow [13]. Once aggregates are formed, we can then superimpose a harmonic oscillation at the tank wall to create dynamic shear within the fluid inside of the tank, thus exposing aggregates to shear without having to remove or manipulate the particles themselves. This allows very fragile flocs typical of the marine environment to be studied. The tank's optical transparency also permits imaging of the flocs using high-speed cameras and laser illumination to capture individual breakup processes. By optically tracking the position of each aggregate as a function of time, we can determine the exact time and position within the tank that causes breakup, allowing us to use analytical solutions describing the fluid motion in the tank to determine the shear causing breakup of each aggregate. Combining these advanced optical measurements with particle tracking and image processing algorithms allows us to capture potentially large quantities of particle disaggregation events with unprecedented detail.

In this paper, we use the rotating and oscillating tank to study the disruption behavior of bentonite aggregates. The paper is organized into the following parts. In part 2, we formulate the theoretical velocities and shear rates of flow under a rotating and oscillating boundary condition. In part 3, we describe the methods used in the particle tracking experiments, and in part 4, we present the preliminary aggregate disruption results. In part 5, we discuss conclusions and recommendations for future work.

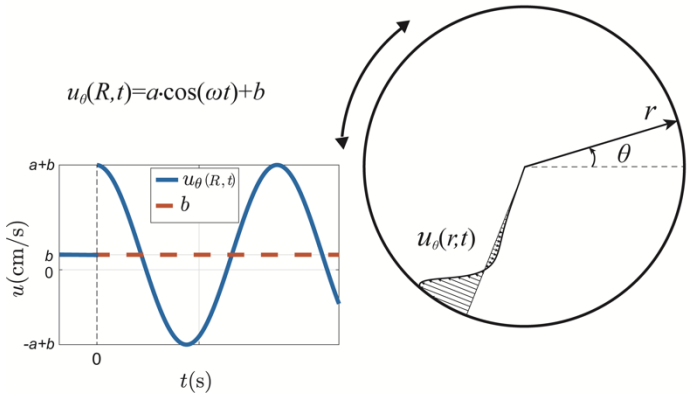

FIGURE 1: Schematic diagram of the fluid region and wall boundary condition of the disaggregation tank.

2. MATHEMATICAL FORMULATION

To derive the theoretical rate of shear throughout the fluid inside of the tank, we assume the rate of rotation or oscillation is small enough that the flow remains laminar. We also assume that salt water is an incompressible Newtonian fluid with a constant kinematic viscosity v. Neglecting pressure, gravitational forces and the effects from both cylinder end walls, the problem simplifies to contain only the azimuthal component of fluid velocity in the Navier Stokes equation. We can thus write the governing equation as,

$$\frac{\partial u_\theta}{\partial t}=v\left(\frac{1}{r}\frac{\partial u_\theta}{\partial r}+\frac{\partial^2 u_\theta}{\partial r^2}-\frac{u_\theta}{r^2}\right) \tag{1}$$

For a cylindrical configuration with only azimuthal velocity, the velocity magnitude at the center of the tank must be zero. Here, we assume that the tank is already in motion at a constant rotation speed prior to the start of the boundary oscillation and the internal fluid, thus, experiences solid body rotation. We can then represent the initial and boundary conditions for this problem as follows,

$$u_\theta(R,t)=a\cdot\cos(\omega t)+b \tag{2a}$$

$$u_\theta(0,t)=0, \tag{2b}$$

$$u_\theta(r,0)=\frac{r}{R}b, \tag{2c}$$

where a and ω are the amplitude and frequency of oscillation, b is the rate of constant rotation at the wall and R is the internal radius of the cylinder. The superposition of the constant rotation rate and oscillation as the boundary condition is shown in Figure 1, where the red dashed line represents the constant rotation rate.

We observe that equation (1) is a linear partial differential equation. Therefore we can decompose the initial and boundary conditions into the homogenous and particular parts. The homogenous part contains only the boundary oscillation, while the particular part represents the solid body rotation. The

homogenous parts of the boundary and initial conditions, equations (2a) and (2c), simplify to

$$u_\theta(R,t)=a\cdot\cos(\omega t), \quad (2d)$$

$$u_\theta(r,0)=0. \quad (2e)$$

The partial differential equation, with homogenous initial and boundary conditions in equations (2b), (2d) and (2e), represent the viscous flow on the inside a cylinder with a harmonic rotation at the wall, the solution to which is provided by the authors [15]. Using this solution, we can calculate the homogeneous part of the quasi-steady fluid velocity as,

$$u_{\theta,H}(r,t)=\frac{a}{2}\left[\exp[i\omega t]\frac{I_1\left(r\sqrt{i\omega/\nu}\right)}{I_1\left(R\sqrt{i\omega/\nu}\right)}+\exp[-i\omega t]\frac{I_1\left(r\sqrt{-i\omega/\nu}\right)}{I_1\left(R\sqrt{-i\omega/\nu}\right)}\right], \quad (3)$$

where I_1 is the modified Bessel function of the first kind and first order. According to the property of linearity, we can apply the method of superposition and simply add the particular solution to the homogenous part, to obtain the velocity profile in this problem. The quasi-steady velocity over time at varying radial distance becomes

$$u_\theta(r,t)=\frac{a}{2}\left[\exp[i\omega t]\frac{I_1\left(r\sqrt{i\omega/\nu}\right)}{I_1\left(R\sqrt{i\omega/\nu}\right)}+\exp[-i\omega t]\frac{I_1\left(r\sqrt{-i\omega/\nu}\right)}{I_1\left(R\sqrt{-i\omega/\nu}\right)}\right]+\frac{r}{R}b. \quad (4)$$

Equation (4) provides the time-varying velocity at different radial positions within the tank once it has reached quasi-steady conditions (*i.e.* after the initial transient at the start of the oscillating motion has decayed). The authors [15] showed that the initial startup transient typically decays within one full cycle of the oscillation. The fluid velocity during this transition from solid body rotation to the quasi-steady velocities can also be calculated using the analytical solution provided in [15]. The right portion of Figure 1 shows the schematic diagram of a snapshot of an example quasi-steady fluid velocity profile. Knowing the fluid velocity, we can calculate the time-varying laminar rate of shear, γ, given as

$$\gamma=r\frac{d(u_\theta/r)}{dr}. \quad (5)$$

Combining equations (4) and (5) allows us to precisely calculate the time-varying shear rate as a function of radial position inside of the tank. We are able to non-dimensionalize the time scale based on the phase of oscillation $\varphi = \omega t$, since the flow motion as a function of the radius is a damped harmonic oscillation. The phase can, thus, be used to determine the magnitude of shear rates.

3. EXPERIMENTAL METHODS

The authors originally developed the experimental breakup facility [14], which is also used here. The facility consists of a transparent cylindrical tank made of acrylic resting on four identical rollers. The tank has a total length of 300 mm, an inner diameter of 100 mm and a wall thickness of 5 mm. A pulley system connects one end of the tank to a programmable motor (Dynamixel MX28-T, Trossen Robotics). The motor has a resolution of 0.114 RPM in angular velocity and 0.88º in angle, which we control using Python. The facility can be rotated at a slow and constant speed to simulate the differential sedimentation aggregation process [13], or oscillated with a boundary condition of the form of equation (2a) to generate fluid shear.

Bentonite clay particles readily form fractal aggregates in saline water. The fragile aggregates also easily break under the influence of fluid shear. Because bentonite flocs have seen previous investigation [2,16], we used bentonite clay particles (Naturalistix Sodium Bentonite Clay) to create aggregates in the oscillating tank facility. To fill the cylindrical tank, we first filled a larger water tank with room-temperature saline water (21 parts per thousand (ppt)), created with tap water and dissolved sea salt (Instant Ocean). We then submerged the open disaggregation tank in the larger tank and injected a solution of suspended bentonite particles through the open end of the cylinder. We quickly fixed the cylinder end cap in place underwater to prevent air bubbles from being trapped within the cylinder. To reach an overall bentonite concentration of 25 mg/L, we dispersed 3.77 g of bentonite clay particles into 300 ml of fresh water using a mechanical mixer. We used a syringe to inject 5 ml of the bentonite solution into the disaggregation tank as described above.

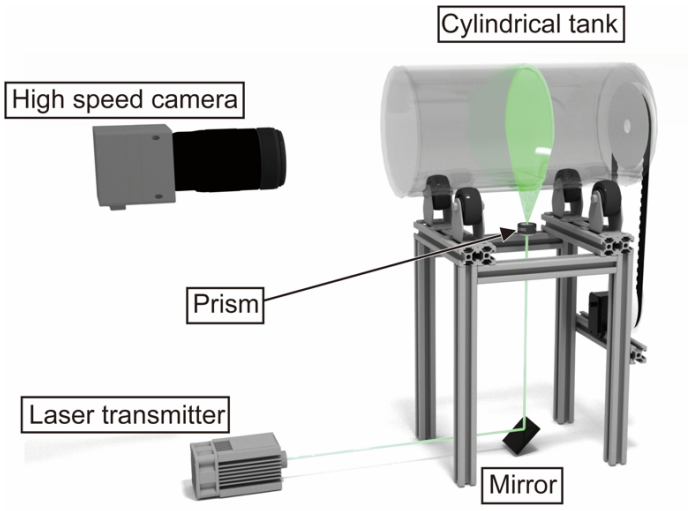

FIGURE 2: Schematic diagram showing the facility and laser path [15].

We created aggregates of by rotating the tank at a constant rate of 2.85 RPM for approximately 4 hours and then observed their size, shape and breakup behavior using a high speed camera and laser illumination. Figure 2 shows the laser path and relative positions of the laser transmitter (Opus 532, Laser Quantum), high speed camera (FASTCAM Mini AX200, Photron) and the test section. The laser had a wavelength of 532 nm and a beam diameter of 1.85 mm. We used a mirror to reflect the laser beam so that it was perpendicular to the tank axis. The beam passed through a Powell lens (75º, Edmund Optics) and a thin slit

aperture to form a laser sheet that bisected the disaggregation tank. The thin slit had a thickness of 0.6 mm to minimize scattering and any diffuse reflections caused by the optical elements and tank wall. This laser sheet geometry illuminated aggregates along a central plane of the tank, allowing their azimuthal motion to be captured with the high speed camera. We observed little out-of-plane particle motion during testing.

The camera viewed the laser sheet through one end of the tank with its viewing axis perpendicular to the laser sheet. We focused the camera using a macro lens with a 200 mm focal length (AF Micro-Nikkor 200mm f/4D IF-ED). A 68 mm extension tube installed between the camera and the macro lens increased the magnification of the field of view (FOV). We estimated the FOV to be 13.5 mm × 13.5 mm (13 μm per pixel resolution with the 1024 × 1024 pixel sensor of the camera). Because this FOV was small and we were most interested on the breakup of aggregates near the tank wall, we positioned the FOV near the bottom tank wall, as shown in Figure 3(b). We recorded image frames as a time series at a rate of 500 fps with a shutter speed of 1/1000 s. We recorded 21,840 image frames for each experiment, which was equivalent to 43.7 s, 6.95 cycles in total.

To determine the fluid velocity and rate of shear for a specific particle breakup event, we need to know both the position and time at which that breakup event occurred. To determine the radial position within the FOV, we used the tank wall visible in each experimental image. In Figure 3(b), a narrow curve of bright light is shown within the dashed box near the bottom of the FOV. This curve is the laser light sheet scattering from the inner wall of the cylindrical tank, which we used to calculate the relative position of the particles. Figure 3(a) shows the fitting process for this calculation, also used previously by the authors [15]. We first extracted the illuminated points along the inner wall of the cylinder. By assuming a uniform circle with a radius equivalent to that of the tank, we then fit this circle to these illuminated points and assumed that the x and y position of the center of the circle coincided with the center of the tank (r = 0). We then used these center coordinates and the position of the wall to calculate the radial locations within the FOV. In this study, we quantified particle sizes by fitting an ellipse to the particle images using Matlab. In the following sections, we report major and minor axis lengths.

To determine the time of each recorded image, we carefully synchronized the high speed camera recording to the tank oscillation. We defined the starting point (t = 0 s) as the time when the disaggregation tank oscillation began. To do this, we triggered the camera to record image frames at the instant the oscillating boundary condition started. We could then determine the time of each recording based on the image number and frame rate.

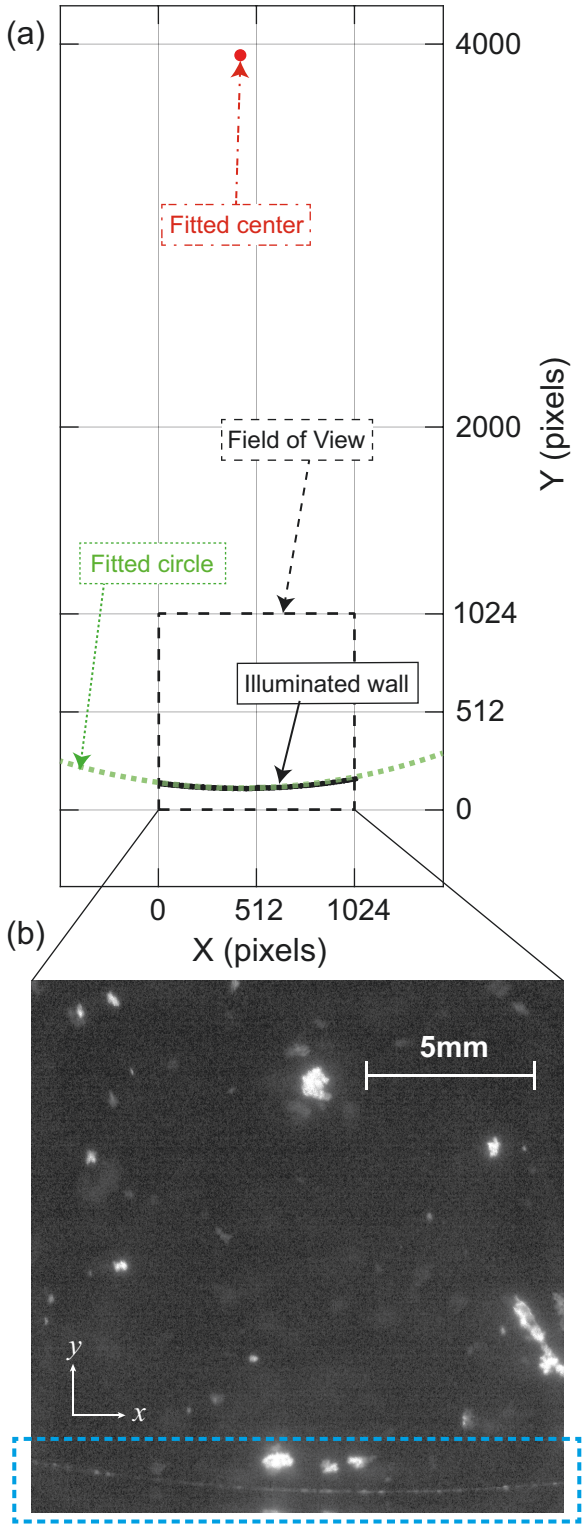

FIGURE 3: (a) The center of the cylindrical tank as determined from fitting a circle to the tank wall within the camera FOV and, (b) the illuminated bentonite aggregates and inner wall of the tank within the camera FOV.

4. RESULTS AND DISCUSSION

4.1 Shear rates inside the tank

In this experiment, the boundary condition at the wall was given as

$$u_\theta(R,t)=9\cos(0.5t)+1.5 \text{ cm/s} \quad (6)$$

where the inner radius of disaggregation tank was $R = 5$ cm. The density of the room-temperature salt water (20.9 ºC, 21 ppt) was $1.01\cdot10^3$ kg/m^3 and the kinematic viscosity was $1.01\cdot10^{-6}$ m^2/s, based on the salinity and temperature of the water. The analytical velocity profile for this boundary condition is the same as the numerical calculation shown previously by the authors [14]. The maximum shear rate for this condition is 61.4 s^{-1}, though this can be adjusted by increasing the oscillation frequency or manufacturing a cylindrical tank with a larger size.

The shear rates obtained by our facility are shown in Figure 4. Similar to the velocity, the shear rates also have a periodic profile. The red line in Figure 4 shows the maximum shear rates as a function of radius while the blue dots are the instantaneous shear rates at a phase angle $\varphi = \pi/2$. The shaded part of the plot represents the range of shear rates in the ocean as discussed above, where the shear rate γ near the mixed layer can reach up to 300 s^{-1}.

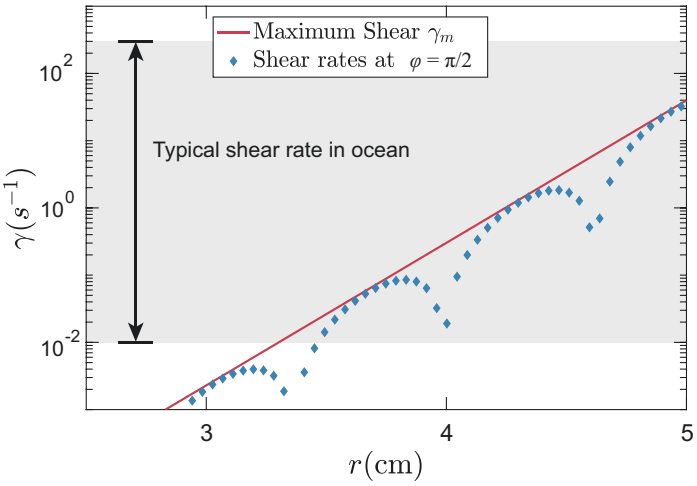

FIGURE 4: Theoretical maximum shear rates as a function of radius in this experiment.

The region of highest shear is close to the wall of tank. Comparing the gray area and the red line in Figure 4, we can see that this region has shear magnitudes similar to the mixed layer near the ocean surface. When the radial distance is less than 3 cm, shear rates are small and we can assume the flocs in this region do not disrupt.

4.2 Characterization of breakup

We observed the breakup of single aggregates during the quasi-steady state motion and during the transient transition from solid body rotation to the new quasi-steady state. Figure 5 shows one example of breakup during the quasi-steady state, where shear forces near the wall deformed and then ruptured one

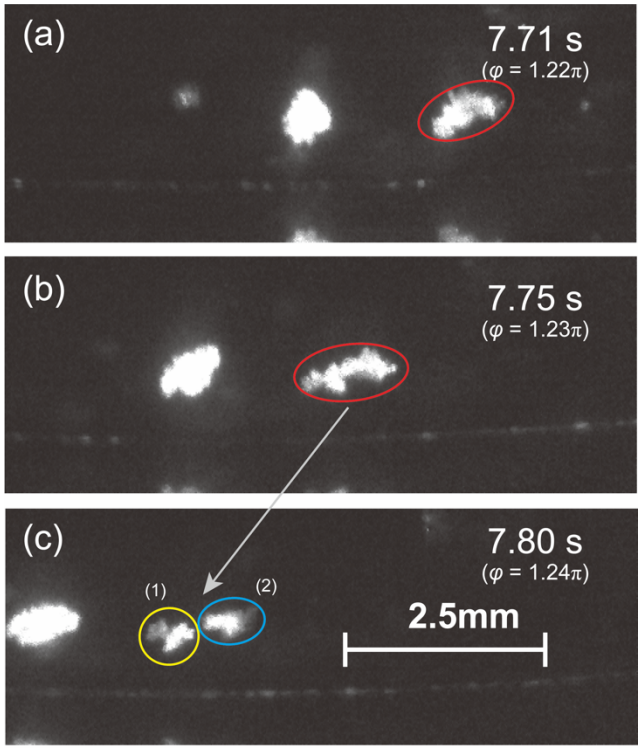

FIGURE 5: The breakup of a single aggregate into two daughter aggregates during quasi-steady state conditions.

aggregate. The aggregate size was small in the original FOV so Figure 5 displays a zoomed-in view. For reference, one full period of oscillation at these conditions is equal to 12.6 s, meaning that the shear magnitude varies with a period of 6.28 s (*i.e.* half of the period of oscillation). We can assume the flow reaches a quasi-steady state after one half period of oscillation [15].

In the first time frame $t = 7.71$ s (Figure 5(a)), we observed two aggregates. The right-most aggregate had a major axis of 765 µm and a minor axis of 338 µm, as determined by fitting an ellipse to the aggregate image. After 0.04 s (Figure 5(b)), the aggregate elongated along its major axis, extending to 1,010 µm. The minor axis, as a result of this stretching, reduced to 270 µm. Figure 5(c) then shows that this aggregate ruptured at $t = 7.80$ s, becoming two daughter sub-aggregates, labeled (1) and (2) in Figure 5(c). The size of the sub-aggregates were roughly the same, with major- and minor- axes of 484 µm × 259 µm and 529 µm × 236 µm. However, due to the limitation of this facility, we could not estimate the out-of-plane thickness or volume of the aggregate.

We calculated the radial position of this aggregate undergoing breakup by its geometric center. It was 4.93 cm away from the center of the tank. Based on this position and the phase angle of the disruption event in Figure 5(c), we estimated the shear rate that caused this breakup to be 14.9 s^{-1} based on equation (5). Interestingly, the other (left-most) aggregate shown

in Figure 5(a-c) does not disrupt despite it being a similar size and experiencing a similar shear to that of the disrupting aggregate.

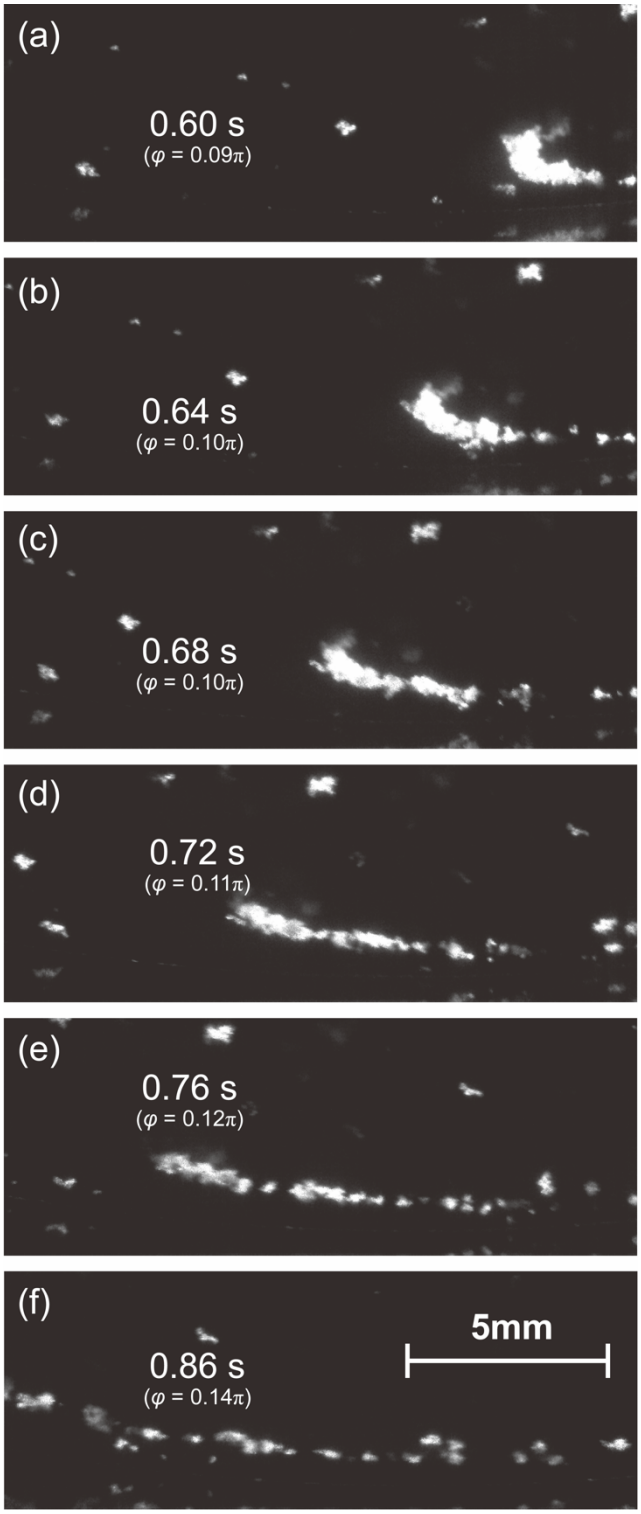

FIGURE 6: The breakup of a very large aggregate into many sub-aggregates during the transition to oscillatory conditions.

Figure 6 shows the breakup of a large aggregate during the transient motion that occurred just as the tank oscillation started. The large aggregate disrupted into many sub-aggregates, leaving a trail of fragments from t = 0.60 s to 0.86 s. We determined the size of this aggregate as it entered the FOV in Figure 6(a) by fitting an ellipse to the aggregate image. The major axis was initially 2,160 μm with the minor axis 1,260 μm. Because there was no radial shear stress in this flow configuration, the azimuthal shear quickly elongated the aggregate and shortened the minor axis, as shown in Figure 6(b) and (c). In this case, the aggregate was not strong enough to maintain plastic deformation under the imposed shear field. As a result, small fragments started breaking off, as shown in Figure 6(b-f). Once the original large aggregate had completely fragmented, all remaining sub-aggregates, shown in Figure 6(f), had a similar size of approximately 117 μm long. We estimated the location of this disruption in Figure 6 to be 4.96 cm away from the center, calculated from the geometric center of the large aggregate. The shear rate increased from 28.4 s^{-1} in Figure 6(b) to 34.7 s^{-1} in Figure 6(f).

During experimentation, aggregates tended to break apart more readily during the startup period of the oscillation than during the quasi-steady oscillation as the shear rates were much greater during this transition. This is also evident by comparing the breakup event of one aggregate into two in Figure 5 to the total fragmentation of a large aggregate in Figure 6. Before the oscillation began, aggregation through solid body rotation produced aggregates with a wide range of sizes. However, the largest aggregates in the flow typically could not survive the transition from solid body rotation to the quasi-steady oscillation. As a result, we plan to pursue more-gentle transitions between the two states so that the breakup behavior of the largest aggregates can be studied.

4.3 Observation of aggregation

One difficulty of studying particle disaggregation is that aggregation and disaggregation both occur due to fluid shear. We did observe aggregation of small particles during the breakup experiment. Figure 7 shows the aggregation of two sub-aggregates. The two sub-aggregates, labeled (1) and (2) in Figure 7(a), were initially very close to each other in Figure 7(a) and similar in size. Their major axes were 475 μm and 422 μm and their minor axes were 277 μm and 237 μm, respectively. In Figure 7(b), they came into contact due to a small difference in azimuthal velocity. We observed that both sub-aggregates also had slightly different angular velocities, which they maintained until they were fully connected. In Figure 7(d), they started to share the same rate of rotation and we considered this moment as the completion of this aggregation event. The newly formed aggregate had a size of 685 μm by 542 μm. At the average radial position of the two sub-aggregates, they were exposed to a shear rate of 0.33 s^{-1}, which is much lower than the shear rates needed to cause the breakup events that were shown in Figure 5 and 6.

There are three main mechanisms to form marine aggregates, Brownian motion, shear contact and differential sedimentation [17]. Traditional aggregation tanks only include

differential sedimentation through solid body rotation [13]. Figure 7 shows that this rotating and oscillating facility can make aggregates from fluid shear in addition to causing breakup. Similar to the process of differential sedimentation, the aggregation due to fluid shear starts from a collision. When two or more sub-aggregates have a small enough difference in velocities and rotation rates, they collide such that surface forces can bond them together, creating one larger aggregate.

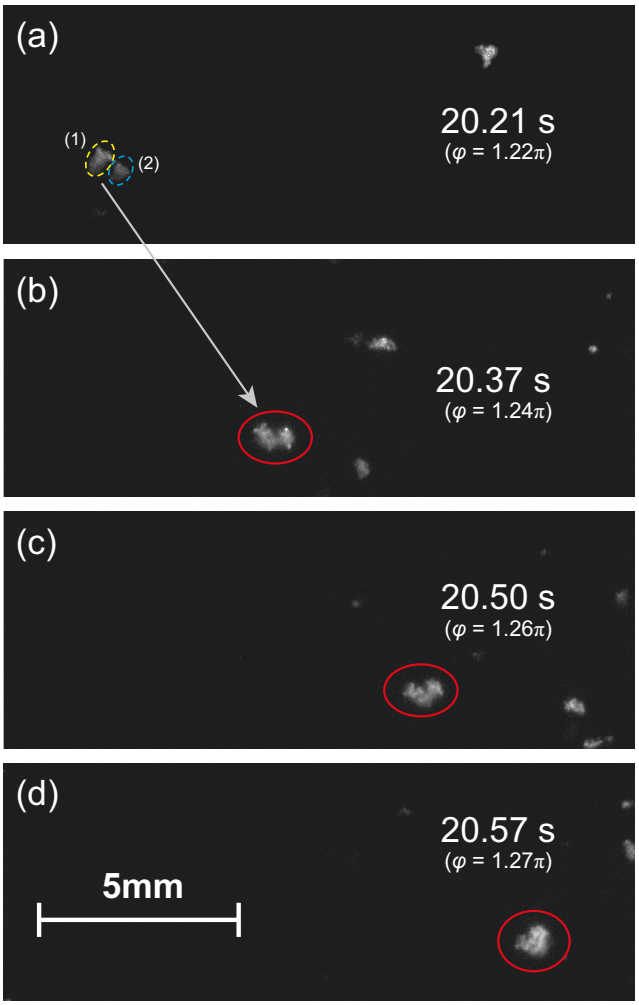

FIGURE 7: Aggregation of two smaller particles and the plastic deformation of the aggregate.

5. CONCLUSION AND FUTURE WORK

We present a rotating and oscillating tank to study the breakup of aggregated marine particulate matter. This novel disaggregation tank provides a range of laminar shear rates that are relevant to the ocean, with the maximum shear capabilities similar to those observed near the ocean surface due to turbulence. By tracking particle positions as a function of time, we can determine the shear rate that causes specific disruption events using the analytical solution of a viscous flow inside an oscillating cylinder.

However, a few open questions remain. The facility likely does not capture the length and time scales of turbulence observed in the natural environment. Additionally, aggregate elongation may play an important role during breakup. To further refine this experiment, we plan to develop algorithms to automatically detect events of aggregate elongation and breakup in large image datasets so that they can be statistically analyzed in the context of naturally-occurring ocean turbulence. We will also expand our particle material types to include additional inorganic and organic marine particles to best represent aggregates of relevance to coastal- and open-ocean regions. These capabilities will allow us to build a large database of aggregate disruption parameters for future modeling efforts.

ACKNOWLEDGEMENTS

The authors would like to thank Dr. Margaret Byron for her assistance with our experimental facility.

REFERENCES

[1] McCave, I. N., 1984, "Erosion, Transport and Deposition of Fine-Grained Marine Sediments," Geol. Soc. Spec. Publ., **15**, pp. 35–69.

[2] Rau, M. J., Ackleson, S. G., and Smith, G. B., 2018, "Effects of Turbulent Aggregation on Clay Floc Breakup and Implications for the Oceanic Environment," PLoS One, **13**(12).

[3] Tambo, N., and Hozumi, H., 1979, "Physical Characteristics of Flocs-II. Strength of Floc," Water Res., **13**(5), pp. 421–427.

[4] Tomi, D. T., and Bagster, D. F., 1980, "Behaviour of Aggregates in Stirred Vessels," Miner. Sci. Eng., **56**(1), pp. 9–18.

[5] Thorpe, S. A., 2005, *The Turbulent Ocean*.

[6] Jiang, Q., and Logan, B. E., 1991, "Fractal Dimensions of Aggregates Determined from Steady-State Size Distributions," Environ. Sci. Technol., **25**(12), pp. 2031–2038.

[7] Saha, D., Babler, M. U., Holzner, M., Soos, M., Lüthi, B., Liberzon, A., and Kinzelbach, W., 2016, "Breakup of Finite-Size Colloidal Aggregates in Turbulent Flow Investigated by Three-Dimensional (3D) Particle Tracking Velocimetry," Langmuir, **32**(1), pp. 55–65.

[8] Zhang, Y., Gao, Z., Li, Z., and Derksen, J. J., 2017, "Transitional Flow in a Rushton Turbine Stirred Tank," AIChE J., **63**(8), pp. 3610–3623.

[9] Wu, H., and Patterson, G. K., 1989, "Laser-Doppler Measurements of Turbulent-Flow Parameters in a Stirred Mixer," Chem. Eng. Sci., **44**(10), pp. 2207–2221.

[10] Alldredge, A. L., Granata, T. C., Gotschalk, C. C., and Dickey, T. D., 1990, "The Physical Strength of Marine Snow and Its Implications for Particle Disaggregation in the Ocean," Limnol. Oceanogr., **35**(7), pp. 1415–1428.

[11] Van Gils, D. P. M., Bruggert, G. W., Lathrop, D. P., Sun, C., and Lohse, D., 2011, "The Twente Turbulent Taylor-Couette (T3C) Facility: Strongly Turbulent (Multiphase) Flow between Two Independently Rotating Cylinders,"

Rev. Sci. Instrum., **82**(2).

[12] Jackson, G. A., 2015, "Coagulation in a Rotating Cylinder," Limnol. Oceanogr. Methods, **13**(4), pp. 194–201.

[13] Shanks, A. L., and Edmondson, E. W., 1989, "Laboratory-Made Artificial Marine Snow: A Biological Model of the Real Thing," Mar. Biol., **101**(4), pp. 463–470.

[14] Song, Y., and Rau, M. J., 2019, "Characterization of Aggregate Disruption Using Organic Marine Particles and Particle Tracking Measurements in Rotating/Oscillating Aggregation Tanks," *Proceedings of the ASME-JSME-KSME Joing Fluids Engineering Conference, San Francisco, California, USA, 28 July - 1 August 2019*, pp. 1–7.

[15] Song, Y., and Rau, M. J., 2020, "Viscous Fluid Flow inside an Oscillating Cylinder and Its Extension to Stokes' Second Problem," Phys. Fluids. (Manuscript submitted for publication.)

[16] Bouyer, D., Line, A., Cockx, A., and Do-Quang, Z., 2001, "Experimental Analysis of Floc Size Distribution and Hydrodynamics in a Jar-Test," Chem. Eng. Res. Des., **79**(8), pp. 1017–1024.

[17] Jackson, G. A., 1994, "Particle Trajectories in a Rotating Cylinder: Implications for Aggregation Incubations," Deep. Res. Part I, **41**(3), pp. 429–437.